

Enhancing and calibrating a goniophotometer

Peter Apian-Bennewitz, Jochen von der Hardt
Fraunhofer Institute for Solar Energy Systems
D-79100 Freiburg, Olmannsstrasse 5, Germany

ABSTRACT

A device for measuring light scattering distribution, a goniophotometer, was improved with new detector geometry and faster data acquisition, and validations of the accuracy were made: The detector linearity was verified with a liquid variable absorber and angular positions using a diffraction grating. The angular resolved scattering data were numerically integrated to be compared with integrating spheres. For this a new integration method uses Voronoi cells on a sphere to integrate arbitrarily located data points, using adaptively refined angular resolution of the measured scattering data. This links the bidirectional-reflection-transmission-function (BRTF) of goniophotometers with the direct-hemispherical transmittance values typically given by integrating spheres.

Keywords: goniophotometer, BRTF, angular resolved scattering measurements, Voronoi cells, two-dimensional numerical integration

1. INTRODUCTION

On the scale of geometrical optics the light field is described by the *radiance* $\mathcal{L}(\vec{x}, \vec{\xi})$ specifying how much power is radiated from a surface element at $\vec{\xi}$ in a given direction \vec{x} . With this, the scattering of light on a macroscopic scale is described by the "bidirectional reflection/transmission function" (*BRTF*), which specifies how much of the incident light distribution \mathcal{L}_{in} is scattered by an infinitesimal surface in a given outgoing direction \vec{x}_{out} . Its implicit definition is given by: *

$$\mathcal{L}_{out}(\vec{x}_{out}) = \int_{\vec{x}_{in}}^{\Omega_{in}=4\pi} BRTF(\vec{x}_{out}, \vec{x}_{in}) \mathcal{L}_{in}(\vec{x}_{in}) \cos(\alpha_{in}) d\Omega_{in} \quad (1)$$

where α_{in} is the angle between the surface normal and the incident direction and the solid angle of integration is 4π , including both reflection and transmission. *BRTF* values are not limited to $[0, 1]$, but extend $[0, \infty]$. Standard measurements of the *BRTF* consist of approximating \mathcal{L}_{in} to a δ -function by using 'parallel' light from a direction \vec{x}_{in} and writing explicitly and *mathematically* correctly

$$BRTF(\vec{x}_{out}, \vec{x}_{in}) = \mathcal{L}_{out}(\vec{x}_{out}) / \mathcal{E}_{parallel} \quad (2)$$

where $\mathcal{E}_{parallel}$ is the incident irradiance. A *measured BRTF* however is inevitably averaged over finite solid angles of the light source ($\Delta\Omega_{in}$) and detector ($\Delta\Omega_{out}$). While this problem is also encountered with other physical quantities like 'velocity', it is particularly significant in *BRTF* measurements because the *BRTF* of samples with high specular transmittance is nearly a δ -function itself and narrower than the angular resolution of the apparatus. Thus the measured *BRTF* depends on the sample *and* on the instrument parameters ($\Delta\Omega_{out}$, $\Delta\Omega_{in}$, see also section 2.1.).

The *BRTF* contains the maximum information on the scattering, with other transmittance values following by integration. The direct-hemispherical transmittance is:

$$\tau_{dh}(\vec{x}_{in}) = \int_{\vec{x}_{out}}^{2\pi} BRTF(\vec{x}_{out}, \vec{x}_{in}) \cos(\alpha_{out}) d\Omega_{out} \quad (3)$$

WWW information available from <http://www.ise.fhg.de/radiance/Welcome.html>

*This notation specifies a two-dimensional integral over the sphere with the integration variable \vec{x}_{in} .

Section 3.2.gives a numerical integration technique for (3). A standard textbook for reflection measurements is for example [1], with original definitions given in [2] and discussions for transmission measurements and ray-tracing contained in [3]. A non-standard way to reverse the convolution in (1) numerically is given in [4].

We start with the enhancements of hardware and measurement procedures which resulted from some years of experience with the former design [5] and diploma work [6] refurbishing the apparatus. The next sections cover test measurements and examples.

2. HARDWARE ENHANCEMENTS

2.1. Xenon lamp

Although $\Delta\Omega_{out}$, $\Delta\Omega_{in}$ could be made fairly small (see section 1), giving a high angular resolution using high quality laser optics [1], it was not the primary goal in this setup. Using a laser as the light source is appropriate for specular materials, but for materials having a broad, low *BRTF*, the total emitted laser power makes the detector signal small. The apparatus requires a fast detector, since it should cover the whole hemisphere in a reasonable time, but a fast *and* very sensitive detector requires unnecessarily sophisticated techniques. Using a 1kW xenon lamp (XBO 1000 manufactured by Osram) offers compromises between signal strength and angular resolution (see fig. 1) by varying diaphragms in the beam path. To check \mathcal{L}_{in} at the sample centre for a given set of diaphragms, a 2mm pinhole was mounted as sample, and its *BRTF* taken as indicator for the angular distribution of the incident light. Fig.2 shows \mathcal{L}_{in} for two different lens diaphragms (diameters 14mm and 30mm). The diameter of the illuminated area **A** at the sample was 25mm.

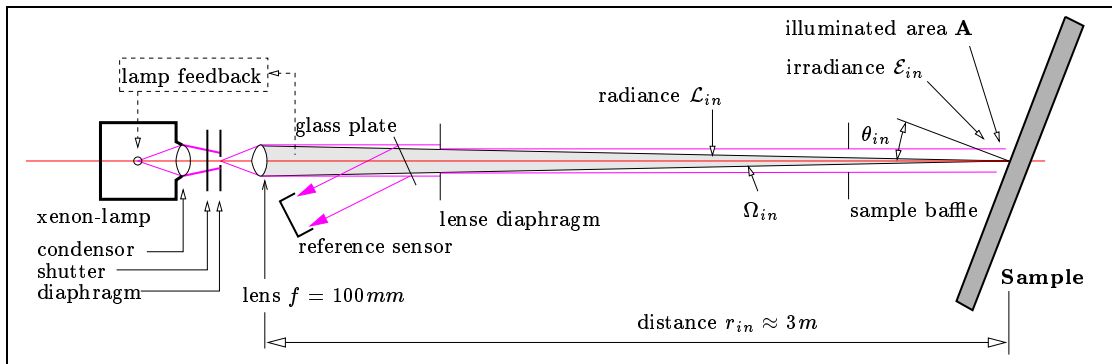


Figure 1. Light source used for small ($3 \times 3 \text{cm}^2$) samples

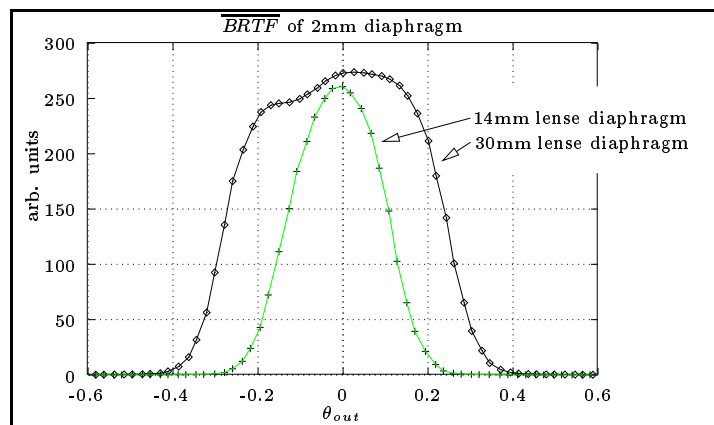


Figure 2. \mathcal{L}_{in} at the sample centre for two lens diaphragms

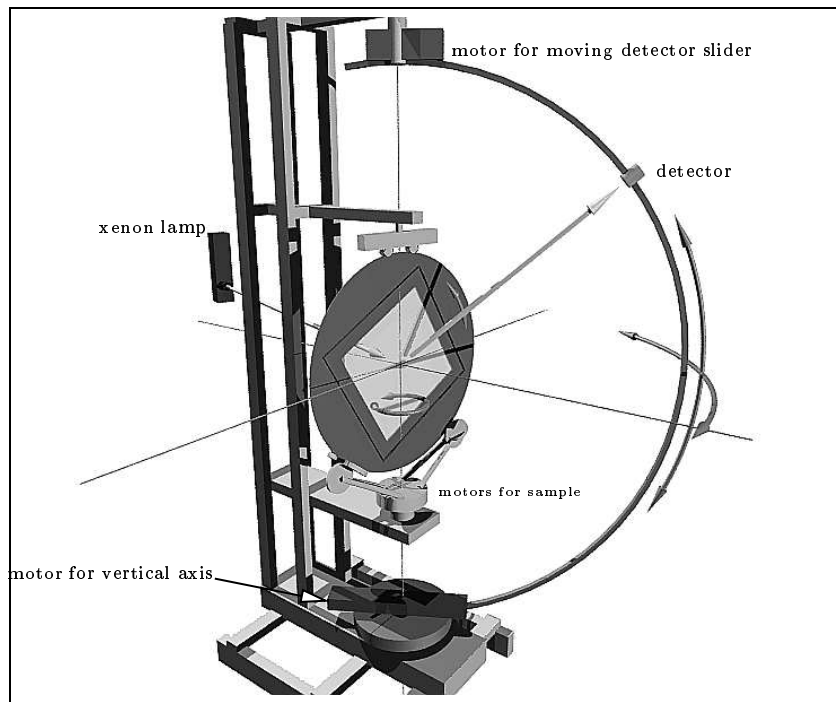


Figure 3. Computer generated perspective view of apparatus

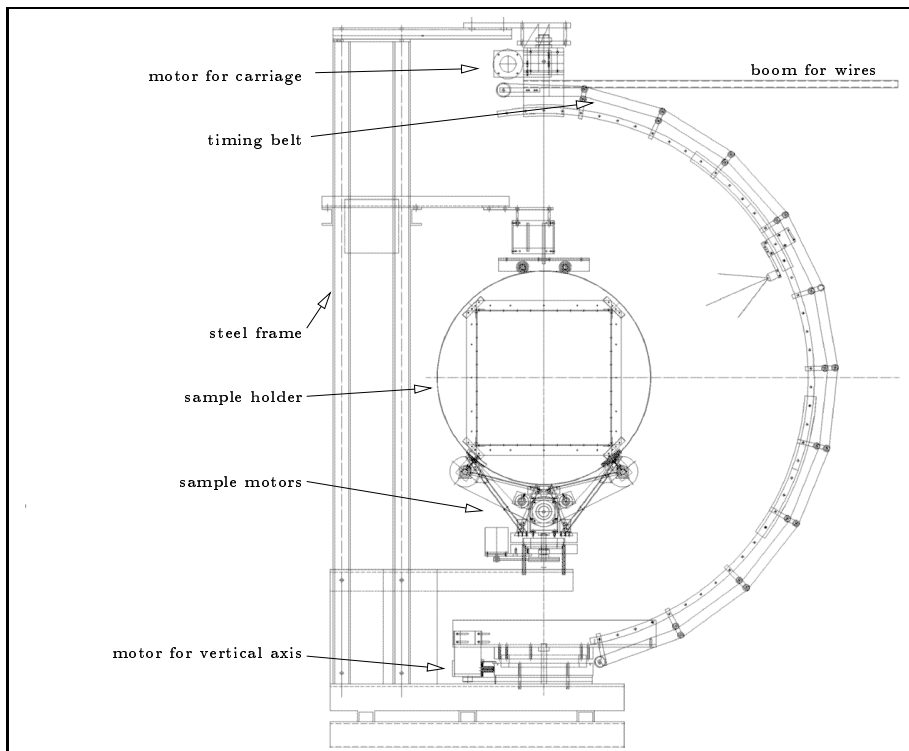


Figure 4. Blueprint of goniophotometer (total height 2.7m)

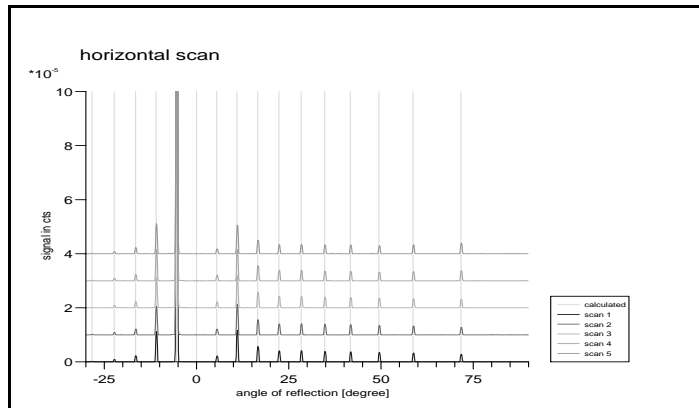


Figure 5. Theoretical positions of 1st-10th order and successive position measurements

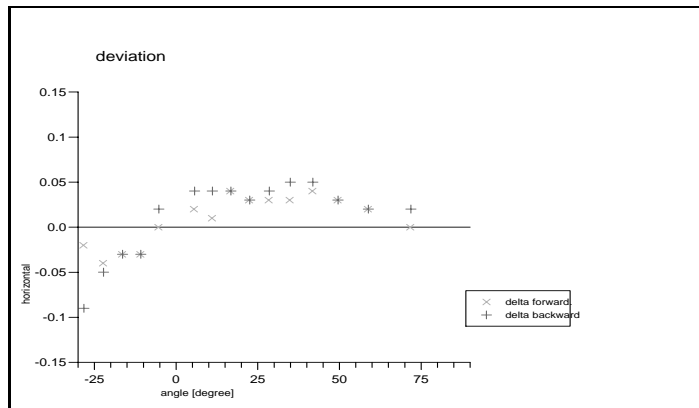


Figure 6. Deviation in horizontal detector position (vertical axis)

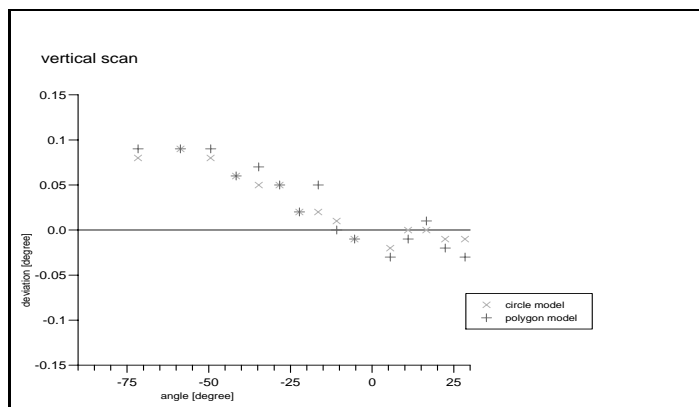


Figure 7. Deviation in vertical detector position (horizontal axis)

2.2. Detector rail

The previous linear detector rail made of two parallel ground steel shafts [5] was replaced by a radial, ground, three-segment steel rail of 1m radius (type HCR made by THK Ltd, see Fig. 3 and Fig. 4). These 60°-segments became available in standard sizes during 1994, and are joined with aluminum 'beds'. Although the first design called for an additional support structure, the stiffness and low weight of the steel rails made them self-supporting, with the upper and lower vertical attachments taking the weight. As with the original design, a 6m long timing belt driven by a stepper motor moves the slider along the rail (see fig. 4). Ten support wheels give the belt a polygonal shape, with a theoretical angular error for the slide position due to polygonalization of less than 1.2'. This is larger than the resolution of the stepper-motor (0.16' per step), but negligible compared to the optical resolution of a standard measurement.

The change of the rail design was motivated by two reasons we learned from the first design: 1. Correcting for different sample-detector distances assumes an exact subtraction of a constant background in the detector signal. This is hardly ever satisfied precisely and multiplying the detector signal by the position-dependent correction factor introduces artificial gradients to the measurements. 2. The mechanical advantage gained by limiting the detector scanning field to a quarter sphere does not compensate for the alignment necessary when using two lamps [3] [7].

2.3. Data acquisition

The current of a silicon diode (type SSO-PD-100 manufactured by Silicon-Sensor) is converted to voltage by a two-step operational amplifier with a switchable resistance in the feedback circuits (type P-9202 made by Gigahertz-Optik in D-82178 Puchheim). The resistors are switched by optically isolated TTL signals and provide a current range from 10^{-10} A to 10^{-2} A in 8 ranges. The output signal is a DC voltage ranging from 0 to 10V which is fed via coaxial cable to an HP34401A multimeter, converting $4\frac{1}{2}$ digits continuously with 10 readings/sec. As in the previous set-up, this data is then transferred via a GPIB interface to the controlling workstation. The increased sampling rate relates directly to an increased angular resolution for the same measurement time, as described in [5], since the detector is moved at constant speed while the data is gathered.

A green $V(\lambda)$ -filter clips the IR response of the photodiode, defining a photometric[†] spectral response for the lamp/detector system. Interchangeable diaphragms mounted in front of the sensor adjust both the view angle which the detector 'sees' of the sample, and the solid angle the detector area subtends relative to the sample centre. Currently the detector 'sees' all luminous sample area. With the standard diaphragm of 5mm diameter, the detector opening angle is 0.28° and subtends a solid angle of $2 \cdot 10^{-5}$ sr.

In the previous design, an internal feedback circuit was used to stabilize the xenon-lamp output, with a small sensor monitoring the beam. Nevertheless, the data showed fluctuations, which, due to the scanning route of the detector, were evident as 'grooves' in plotted data. This was traced to lamp fluctuations on the order of minutes, not compensated by the feedback circuit. Either the feedback was at fault, or it is insufficient to stabilize the beam at *one* spatial position, when the beam profile changes due to the xenon arc 'jumping'. The feedback circuit was removed and a reference solar-cell added, which receives 10% of the beam reflected by a 10^0 off-normal glass plate and integrates over the beam profile. The reference signal is acquired by an HP34401A multimeter operating as an ammeter and read synchronously with the detector signal. For later reference, it is also stored in the data file.

2.4. Checking angular position

All axes were aligned relative to each other during assembly of the goniophotometer using 'geometric' methods (large scale verniers, plummet, levelling laser). Although it is easy to calculate the mechanical resolution of the stepper motors in degrees per step, the question remained as to whether the detector is actually in the calculated position relative to the sample and to the light source. Systematic position errors of the detector or the sample include angular misalignment of axis or offsets between axis. The detector rail might also bend under its own weight. Furthermore, the backlash between the motor axis and the detector vertical axis has to be measured once to be corrected in software for 'normal' measurements.

As described in [7], two main axes are defined for the goniophotometer: A vertical axis, defined by a precision plummet, and a horizontal axis defined by a wall-mounted laser aligned with a water-level. Both axes pass through the sample centre. The sample holder is checked using reflections from a sample mirror, yielding an accuracy $< 0.4^\circ$.

[†]Nevertheless radiometric terminology is used in this text for convenience.

For testing the detector position, a grating (150 lines/mm, grazed) was mounted as a sample, and the measured peak locations compared to calculated positions as shown in Fig. 5. The laser was used as the light source and the grating was aligned to retroreflect. By rotating it around the vertical sample axis the front surface was checked to be at the sample centre, as otherwise geometrical deviations would result for the outgoing directions. Each Gaussian-shaped maximum was finely scanned, its maximum found and the deviations from calculated values plotted. Fig. 6 shows measurement results for the vertical axis. The results show that the position of the detector is accurate to at least $\pm 0.1^\circ$, which is sufficient for the measurements currently made.

2.5. Testing the detector's dynamic range

The *BRTF* varies over a large dynamic range: From optically clear samples (e.g. glass plates) to diffusely scattering materials the literature gives a $1 : 10^7$ range [1]. The better the input beam is collimated, the higher the ratio: Light from a small solid angle is scattered into the hemisphere. While measuring the beam as a reference, or samples with a high specular transmittance, the detector moves through the small cone of intense light, giving the maximum signal. With light-diffusing samples, the detector receives only a fraction of the homogeneously scattered light, and the signal is minimum. Some fairly common materials even combine both extremes, like transparent glass panes screen printed with white dots, used for daylight shading. Their *BRTF*, averaged over the sample surface, shows a pronounced peak and a low background. Both are significant for daylight simulations.

Linearity between incident power on the detector and the digitized readout is required and depends on the linearity of the components: response of the silicon cell, current-voltage converter and multimeter. The short circuit current of a silicon cell is linear between saturation illumination and the dark current. The upper limit is not reached with the present lamp configuration and the lower limit, plus electronic noise, defines the lowest measurable *BRTF*. Also of interest were resistances at the converter input and between the cell and converter, which drive the cell out of the ideal short circuit current situation. The converter typically maps the full input current range to a smaller voltage range by selectable resistances in the converter. This was the most questionable component, although new and certified. The voltage multimeter was considered to be non-critical, since a 1V to 10V signal will be accurately digitized.

To test the linearity of the complete data acquisition and avoid secondary effects, the test illumination should be variable and a controllable over eight decades, with constant state of polarization and frequency distribution and spatially constant over the receiving surface. Some possible methods are shown in table 1.

method	advantages	disadvantages
absorption by liquid with varying concentration	cheap & precise	concentration of absorber must satisfy Lambert-Beer law
pair of polarizers	fast, reproducible	very fine angular resolution near 'crossed' position necessary
set of grey filters	cost (photographic filters)	multiple reflections between surfaces
two integrating spheres connected by an aperture of variable diameter. First sphere acts as light source, detector is mounted in second sphere.	depends only on mechanical parameter	low illumination levels at detector
grey step-wedge	compact	only homogeneous over small beam diameter
r^{-2} law	depends only on mechanical parameter	large distance $\approx 20\text{-}50\text{m}$

Table 1. Some methods for varying a reference beam over eight decades

The first method was used with a HeNe laser and a green organic dye dissolved in water: A concentrated solution was fed with a precision pipette (Pipetman P-200 made by Gilson) into a 100mm long, 16mm diameter glass cell

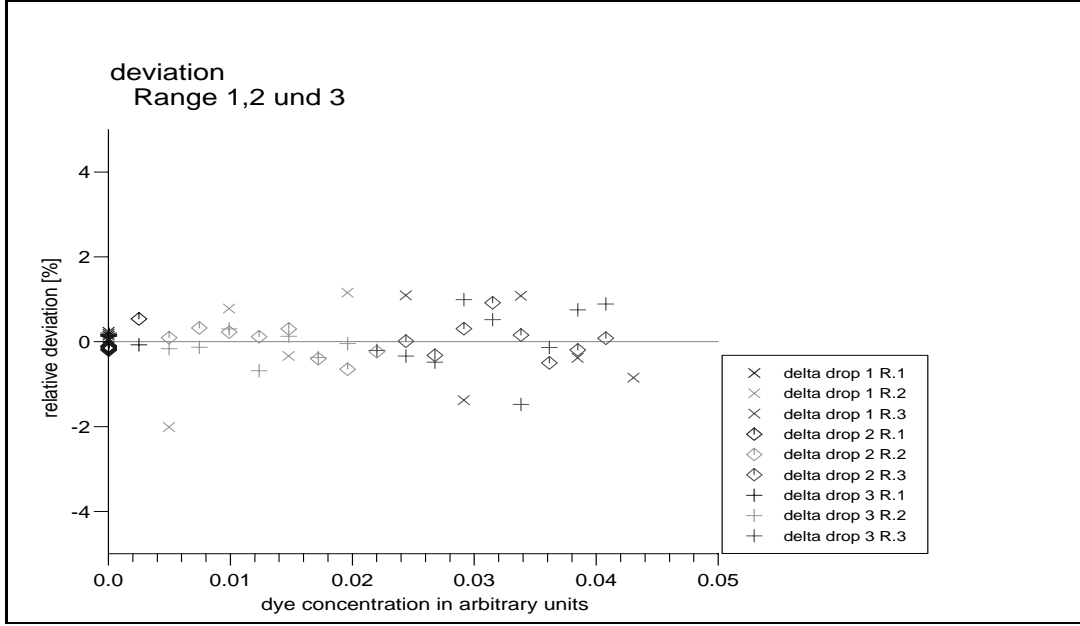


Figure 8. Deviation from Lambert-Beer extinction law versus dye concentration

for spectrometer use. The cell is slightly tilted to avoid multiple reflections between the entry and exit windows. Measurements started from an arbitrary concentration, with a controlled stepwise increase in dye. After stirring the half-full cavity by airflow, the detector signal was read in all current ranges. Systematic deviations from the Lambert-Beer law occurred at high concentrations (low measured intensities), as the measured absorption is below the theoretical, probably due to the dye molecules forming larger particles. The procedure was repeated three times, and fig. 8 shows the deviation from the theoretical absorption. As outlined in [6] the errors are within 3%, giving an upper limit to the linearity error for the detector data acquisition. Statistical in nature, they are due more to errors in the setup, than a non-linear response.

3. DATA PROCESSING AND ANGULAR INTEGRATION

3.1. Beam reference measurement

To obtain absolute $BRTF$ values (2), the measured outgoing radiance distribution is divided by the incident irradiance. Using a second sensor for irradiance would require matching the two detectors and thereby introducing additional errors. However it is simple to use the *same* detector for measuring the beam itself. The current design uses an approach where the $BRTF$ is calculated without requiring exact knowledge of the solid angle of the detector or the beam diameter. Our measurement procedure is then to make 'beam reference scans' with the sample removed every 10th measurement or at least once per set of measurements for one material and set of incident angles. In this way, the second sensor described in section 2.3. is only used to compensate for lamp fluctuations.

For measurements with a sample, it follows from fig. 9 that the radiance emitted from the sample averaged over the detector solid angle is:

$$\mathcal{L}_{average} = \frac{\kappa I r^2}{\mathbf{A}_{Det} \cos(\alpha) \mathbf{E}} \quad (4)$$

where I is current from the cell, κ is a conversion factor and the other geometric quantities are shown in fig. 9. The detector area and sample area are assumed to be small relative to the detector distance, and the $BRTF$ flat enough for the r^{-2} law to hold. Note that the viewing angle of the detector includes the entire luminous sample area, which assumes that this area is about equal to the front illuminated sample area, which holds true only for so called 'optically thin' materials. Other materials (e.g. honeycombs) require a baffle behind the sample or a lens in

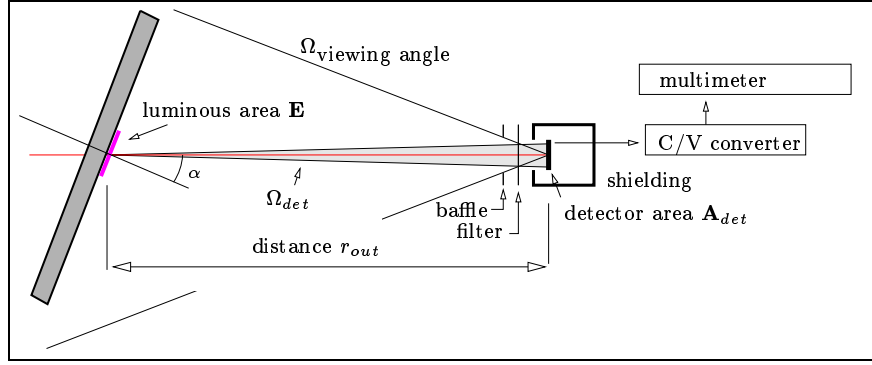


Figure 9. Detector geometry

front of the detector to limit the viewing angle. Also a light source with a larger illumination diameter has to be used in these cases, to ensure an energy balance with regard to the outgoing area.

In measuring the power Φ of the collimated beam, the signal will be proportional to the beam-cross section convoluted with the detector area. Integrating the sampled points of the beam profile the signal Σ is proportional to the detector area \mathbf{A}_{Det} , and the total power contained in the beam is given by:

$$\Phi_{beam} = \frac{\kappa \Sigma}{\mathbf{A}_{Det}}$$

Substituting this into (2) and using $\mathcal{E}_{in} = \Phi_{beam}/\mathbf{E}$, we find:

$$\overline{BRTF}(\vec{x}_{in}, \vec{x}_{out}) = \frac{\overline{\mathcal{L}}_{out}(\vec{x}_{out})}{\mathcal{E}_{in}} = \frac{I(\vec{x}_{out}) r_{out}^2}{\cos(\alpha) \Sigma} \quad (5)$$

where \overline{BRTF} indicates the $BRTF$ averaged over the detector and lamp solid angles (see remarks on eq. (2)). Neither solid angle appears explicitly in the formula, and their exact values are not needed for calculating \overline{BRTF} from the detector currents. The calculation of Σ will be further elaborated in the next section.

3.2. Integration over the hemisphere, direct-hemispherical transmittance τ_{dh}

We need numerical integration in two dimensions for two reasons: The beam profile must be integrated to obtain the total beam power in (5), and the $BRTF$ values need integration to determine the direct-hemispherical transmittance τ_{dh} in (3). For both cases, the angular adaptive refinement method (AARM) [5] measures at points which are arbitrarily located on the hemisphere. We find a common problem in two-dimensional numerical integrals: Each point has to be associated with a surface 'around' it. On a regular grid (see fig. 10), the area A is simply given by the grid constants $A = ab$. This is a special case of the general *Voronoi cell*, defined as all points nearer to a given point than to any other point:

$$\text{Voronoi}(\vec{x}_k) = \{\vec{x} \in \mathbb{R}^n \mid \|\vec{x} - \vec{x}_k\| < \|\vec{x} - \vec{x}_i\|, \forall i \neq k\}$$

A is generally defined as a measure of the Voronoi set (e.g. solid angle for a spherical polygon if Voronoi cells are constructed on a sphere). Numerous $N \log(N)$ algorithms for constructing Voronoi cells from N points in a plane are known (see [3] for a list), but Voronoi cells in a sphere seem somewhat rare. One of us (Jochen von der Hardt) wrote a program to calculate these. One output is shown in fig. 11. The cell size adapts to the spacing of the measurement points, as these are adaptively refined, depending on the measurement signal (a more detailed explanation of the refinement was given in [5]).

Once the Voronoi cells are known, the integration is a sum of the signal times the area of the associated Voronoi cell (Riemann sum) as shown in fig. 12. By this, we are able to compute τ_{dh} from the $BRTF$. Fig. 13 shows a first comparison between numerically integrated τ_{dh} values and measurements done with an integrating sphere. The deviations for the three materials will be further investigated, as to whether systematic errors are due to the integrating sphere or the goniophotometer.

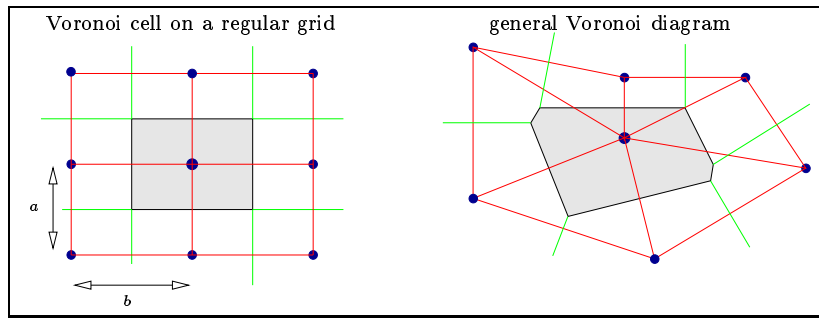


Figure 10. Two examples of Voronoi cells in the plane.

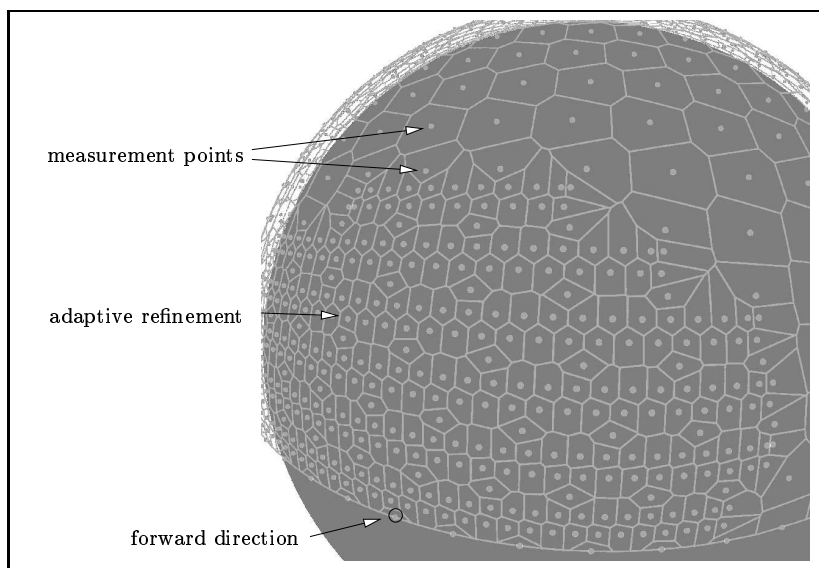


Figure 11. Voronoi cells on a sphere around each measured point. The measured values are not shown in this plot.

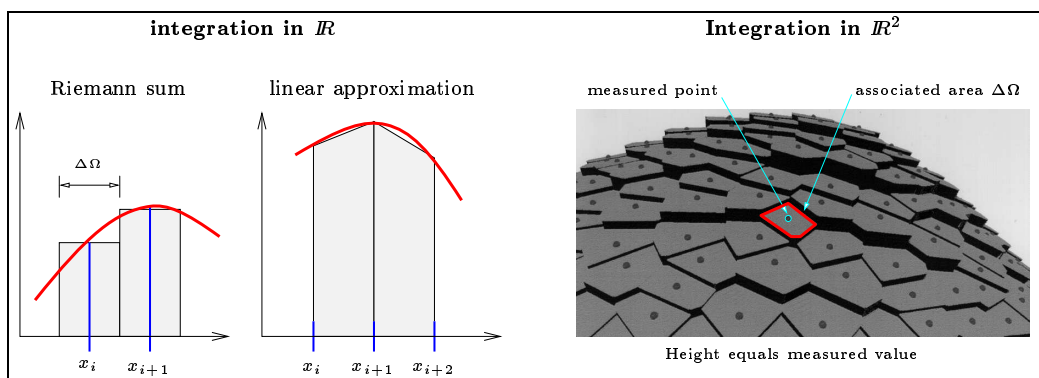


Figure 12. Integration in one and two dimensions: Voronoi cells define $\Delta\Omega$, the area around each point used in a 2d Riemann sum.

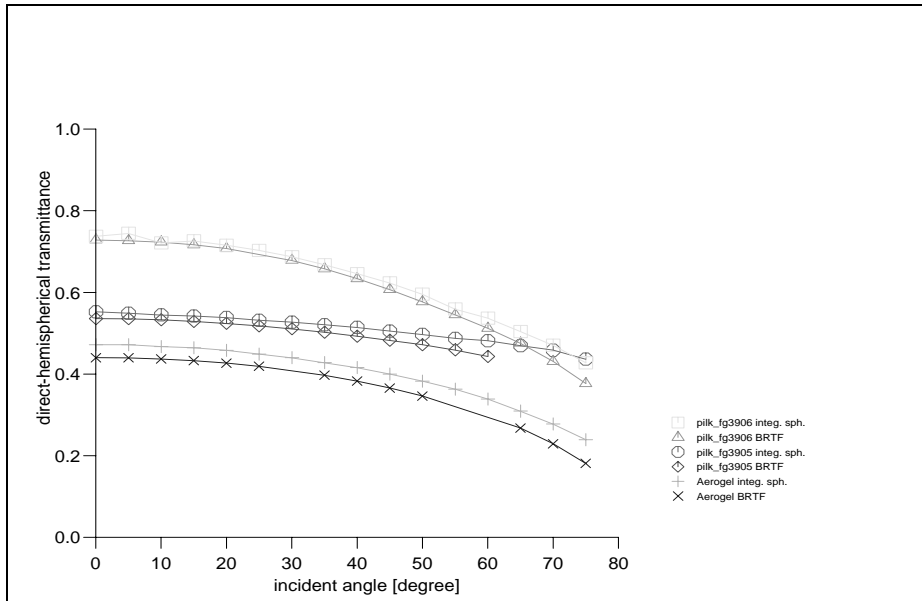


Figure 13. The direct-hemispherical transmittance τ_{dh} measured with an integrating sphere and numerically integrated from *BRTF* data for three materials.

4. DISCUSSION

The changes, tests and procedures aim at increasing confidence in *BRTF* values measured by our goniophotometer. This is distinguished by sufficient mechanical angular accuracy (0.1°), optical resolution, linear response and (for the first time) comparison with a different measurement technique (integrating spheres). For the intended task of the goniophotometer, namely measurement for daylighting simulation, this exceeds the requirements, and allows additional use of the apparatus for material characterization. The test uses 'in-house' methods, which appear to be useful and necessary before doing a round-robin check between goniophotometers, as results tend to scatter [8].

For further details on the measurements see the description in [6]. A discussion of the *BRTF* and transmission quantities can be found in [3], which also details theoretical modelling by ray-tracing methods.

ACKNOWLEDGEMENTS

We wish to thank Dr. Wittwer and the mechanics (Walter Schnetzler, Armin Bösch) for much valuable help and precise engineering. This work was supported by BMBF project 0335004M.

REFERENCES

1. J. C. Stover, *Optical Scattering: Measurement and Analysis*, McGraw-Hill, 1990.
2. ANS, "Standard recommended practice for goniophotometry of objects and materials," Tech. Rep. E167-77, American National Standard, 1977.
3. P. Apian-Bennwitz, *Messung und Modellierung von lichtstreuenden Materialien zur Computer-Simulation von Tageslichtbeleuchtung*. PhD thesis, Universität Freiburg, Fraunhofer Institut für solare Energiesysteme, D-79100 Freiburg, November 1995.
4. T. Schmidt, *Optische Charakterisierung transparenter Materialien in Hinblick auf eine Auswertemethode experimenteller Streudaten*. Master's thesis, Universität Freiburg, Fraunhofer Institut für solare Energiesysteme, D-79100 Freiburg, März 1993.

5. P. Apian-Bennowitz, "Designing an apparatus for measuring bidirectional reflection/transmission," in *Optical Materials Technology for Energy Efficiency and Solar Energy Conversion XIII*, pp. 697–706, SPIE, Vol 2255, April 1994.
6. J. von der Hardt, *Optimierung eines Messverfahrens zur Untersuchung des Streuverhaltens lichtlenkender bzw. -streuender Elemente*. Master's thesis, Universität Freiburg, Fraunhofer Institut für solare Energiesysteme, D-79100 Freiburg, Oktober 1995.
7. P. Apian-Bennowitz, *Bau einer Apparatur zur Messung winkelabhängiger Licht-Streuung an anisotropen Medien*. Master's thesis, Universität Freiburg im Breisgau, April 1990.
8. T. A. Leonard and M. Pantoliano, "Brdf round robin," in *Stray Light and Contamination in Optical Systems*, pp. 226–235, SPIE Vol. 967, 1988.